CrossMark

ORIGINAL PAPER

Using a fully recyclable dicarboxylic acid for producing dispersible and thermally stable cellulose nanomaterials from different cellulosic sources

Chao Jia · Liheng Chen · Ziqiang Shao · Umesh P. Agarwal · Liangbing Hu · J. Y. Zhu

Abstract We fabricated cellulose nanocrystals (CNCs) and cellulose nanofibrils (CNFs) from different cellulose materials (bleached eucalyptus pulp (BEP), spruce dissolving pulp (SDP) and cotton based qualitative filter paper (QFP) using concentrated oxalic acid hydrolysis and subsequent mechanical fibrillation (for CNFs). The process was green as acid can be easily recovered, and the prepared cellulose nanomaterials were carboxylated and thermally stable. In detail, the CNC yield from the different materials was similar. After hydrolysis, the DP of the cellulose materials decreased substantially, whereas the mechanical fibrillation of the cellulosic solid residues (CSRs) did not dramatically reduce the DP of cellulose. CNCs with different aspect ratios were produced from different starting materials by oxalic acid hydrolysis. The CNCs and CNFs obtained from BEP and QFP possessed more uniform dimensions than those from SDP. On the other hand, CNFs derived from SDP presented the best suspension stability. FTIR analyses verified esterification of cellulose by oxalic acid hydrolysis. The results from both XRD and Raman spectroscopy indicated that whereas XRD crystallinity of CNCs from BEP and QFP did not change significantly, there was some change in Raman crystallinity of these samples. Raman spectra of SDP CNCs indicated that the acid hydrolysis preferably removed cellulose I portion of the samples and therefore the CNCs became cellulose II enriched. TGA revealed that the CNCs obtained from QFP exhibited higher thermal stability compared to those from BEP and SDP, and all the CNCs possessed better thermal stability than that of CNCs from sulfuric acid hydrolysis. The excellent properties of prepared cellulose nanomaterials will be conducive to their application in different fields.

C. Jia · Z. Shao
School of Materials Science and Engineering, Beijing Institute of Technology, Beijing 100081, China

C. Jia · L. Hu
Department of Materials Science and Engineering, University of Maryland College Park, College Park, MD 20742, USA

C. Jia · L. Chen · U. P. Agarwal · J. Y. Zhu (✉)
Forest Products Laboratory, USDA Forest Service, Madison, WI 53726, USA
e-mail: jzhu@fs.fed.us

L. Chen
Key Laboratory of Biomaterials of Guangdong Higher Education Institutes, Department of Biomedical Engineering, Jinan University, Guangzhou 510632, China

Introduction

Cellulose, as the most abundant natural polymer on the earth, has received much attention as a carbon resource

(Jonoobi et al. 2015; Kim et al. 2015). It is biodegradable and can be obtained from renewable plants, for example, wood (Mathew et al. 2014), cotton (Beltramino et al. 2015), bamboo (Lu et al. 2014), hemp (Luzi et al. 2014), bacteria [e.g., acetobacter xylinum (Zhang et al. 2014)], marine animals [e.g., tunicates (Sacui et al. 2014; van den Berg et al. 2007)] and algae [e.g., cladophora glomerata (Xiang et al. 2016)]. Among cellulose materials, cellulose nanocrystals (CNCs) and cellulose nanofibrils (CNFs) are particularly attractive because of their unique properties, such as large surface area, high aspect ratio, high Young's modulus, lightweight, abundance, low thermal expansion, optical transparency, renewability, biodegradability and low toxicity. Therefore, they have been applied in various fields. CNCs can be used in polymer reinforcement (Spinella et al. 2015; Xu et al. 2014), antimicrobial materials (de Castro et al. 2016), green catalysts (Cirtiu et al. 2011), responsive photonic hydrogels (Kelly et al. 2013), light-healable supramolecular nanocomposites (Biyani et al. 2013), shape-memory nanocomposites (Mendez et al. 2011), biosensors (Schyrr et al. 2014) and drug delivery (Taheri and Mohammadi 2015). On the other hand, CNFs have applications in biodegradable composites (Eichhorn et al. 2010; Moon et al. 2011), which includes films made of CNFs also called nanopaper for flexible electronic devices, such as phototransistor (Zhang et al. 2016b), touch screen (Zhu et al. 2016), light emitting diode (Xu et al. 2016), and so on. In addition, as reinforcement polymers, CNCs and CNFs showed very different reinforcing effects due to their difference in morphology (Xu et al. 2013).

The most commonly used method for producing CNCs is hydrolysis using concentrated mineral acids, such as sulfuric acid (Chen et al. 2015; Hamad and Hu 2010), hydrochloric acid (Sacui et al. 2014; Yu et al. 2013) and phosphoric acid (Espinosa et al. 2013; Lu et al. 2015). Among them, sulfuric acid hydrolysis is often used to produce CNCs with surface sulfate group to facilitate aqueous dispersion. Unfortunately, the resultant CNCs have poor thermal stability due to the sulfate groups (Roman and Winter 2004; Wang et al. 2007), which limits further processing at elevated temperatures such as in injection molding, twin-screw compounding, and extrusion. CNCs prepared using hydrochloric acid hydrolysis exhibit good thermal stability but tend to aggregate in water. They have poor dispersion due to limited surface charge (Yu et al.

2013). Mineral acid hydrolysis also suffers from problems such as equipment corrosion, difficulties in economic recoveries of acid and dissolved sugars, disposal of a large amount of waste water and salts from acid neutralization, and low yield (Bondeson et al. 2006; Dong et al. 1998; Hamad and Hu 2010) though the yield issue has been addressed recently with CNC yield as high as 90% (Chen et al. 2015; Wang et al. 2012, 2014). TEMPO-mediated oxidation has been widely used for producing CNFs followed by mechanical fibrillation with low energy input (Kurihara and Isogai 2014). It has been reported that the method has been applied for industrial scale production (Peyre et al. 2015). CNFs with high aspect ratios and diverse surface functionalities (carboxyl, aldehyde, and hydroxyl) can be generated. TEMPO, however, is expensive. Economic chemical recovery yet needs to be demonstrated.

An alternative to mineral acids, organic acids have been utilized for CNC production with ultrasonic assistance (Filson and Dawson-Andoh 2009; Tang et al. 2013). In addition, the cellulose hydrolysis by acid mixture of mineral and organic acids has also been used (Braun and Dorgan 2009; Spinella et al. 2015; Yu et al. 2015). These studies did not solve the problems of acid recovery for green processing and improve CNC dispersion, functionalization, and good thermal stability. Recently, we demonstrated integrated production of highly thermal stable and carboxylated (with surface charge) CNCs and CNFs using fully recyclable solid dicarboxylic acid (Bian et al. 2017b; Chen et al. 2016; Wang et al. 2017). Dicarboxylic solid acids often have lower ionization degrees than those of mineral acids, for example, oxalic acid has $pK_{a1} = 1.27$ and $pK_{a2} = 4.28$ at 25 °C, therefore, a more harsh reaction condition is required for CNC production through hydrolysis. Oxalic acid can be produced from natural sources, such as biomass (Guru et al. 2001). It exists in many plants and vegetables, and is also a metabolic product in many fungi (Lacerda et al. 2015). On the other hand, oxalic acid can be readily recovered and reused through a conventional and commercially proven crystallization process at a low or ambient temperature for sustainable and economic manufacturing (Chen et al. 2016).

In this paper, we focus our study on evaluating the susceptibilities of different cellulosic materials, i.e., bleached kraft eucalyptus pulp (BEP), spruce dissolving pulp (SDP), and qualitative filter paper (QFP), to

concentrated oxalic acid hydrolysis for producing CNCs and CNFs at three concentrations. The main objective of this work is to study the effects of oxalic acid concentration and feeding cellulosic material on the key properties of the resultant CNCs and CNFs, including yield, morphology, degree of polymerization (DP), surface charge, etc. In addition, CNCs obtained from the different cellulosic materials were studied by Fourier transformed infrared spectra (FTIR), Raman spectroscopy, X-ray diffraction (XRD) and thermogravimetric analyses (TGA) to compare their chemical structure, crystallinity, and thermal stability.

Experimental

Materials

Anhydrous oxalic acid (98%) and sulfuric acid were purchased from Sigma-Aldrich (St. Louis, MO). All these chemicals of reagent grade were used as received without further treatment.

Bleached kraft eucalyptus dry lap pulp (BEP) was obtained from a commercial source (Fibria, Aracruz Cellulose, Brazil). Macerated (fully) spruce dissolving pulp (SDP) was received from a commercial pulp mill. Native cotton fibers were from qualitative filter paper (QFP, Ahlstrom 617, 0.5207 mm thickness and 122.9 g/m^2, ash content <0.06%) purchased from Ahlstrom (Helsinki, Finland). The chemical compositions of the three cellulosic materials were analyzed (Table 1) by the Analytical Chemistry and Microscopy Lab at the USDA Forest Products Lab.

All the starting materials (Fig. 1a) were first soaked in deionized (DI) water overnight, then the BEP and SDP were disintegrated for 10,000 revolutions at 312 rpm and 2% consistency at room temperature using a laboratory disintegrator (Model 73-06-01, TMI, Ronkonkoma, New York, USA). The resultant pulps were then vacuum dewatered and air dried to approximately 5% moisture content (Fig. 1a). The air dried pulps were used in oxalic acid hydrolysis. QFP was directly used in acid hydrolysis.

Oxalic acid hydrolysis

The preparations of oxalic acid solution for acid hydrolysis experiments was described previously

(Bian et al. 2017b; Chen et al. 2016). The reactor was a 500 mL three-necked round-bottom flask equipped with a condenser, and heated in a glycerol bath (IKA® C-MAG HS 7 digital, Staufen, Germany) at 100 °C. Fibers of 10 g in oven dry (OD) weight were hydrolyzed using fiber to acid solution ratio of 1:10 (w:w). A mechanical stir bar was used for mixing at a speed of 300 rpm during hydrolysis. The reaction was immediately quenched at the end of 1 h hydrolysis by adding 400 mL de-ionized (DI) water into the flask, and then vigorously stirred to disperse the products. The resultant suspension was washed and centrifuged at 10,000 rpm for 10 min (Sorvall RC-5B Plus, Du Pont, Newtown, CT, USA). The centrifugation procedure was repeated three times to remove remaining oxalic acid. The supernatant from the first two centrifugation was collected for carbohydrate analyses. The precipitates from the third centrifugation were diluted with DI water. The solid suspension was then dialyzed using DI water until the conductivity of the liquid approached that of DI water. Upon completion, CNCs were isolated by repeated centrifugation at 10,000 rpm for 10 min. After the collection of the first turbid supernatant, the precipitate was re-suspended and again centrifuged to obtain additional CNCs in the form of a turbid supernatant. The CNCs in the first three turbid supernatants were recovered and combined.

The collected hydrolysate was further hydrolyzed using a 4 wt% sulfuric acid solution at 121 °C for 1 h heated in an oil bath to convert oligosaccharide to monosaccharide. The sugar solution was then neutralized by $CaCO_3$ to a pH of approximately 6. The sugar composition of the solution was analyzed using a high performance liquid chromatography (HPLC) (Ultimate 3000, Thermo Scientific, USA).

Mechanical fibrillation of CSR

The precipitated partially hydrolyzed fibers, called cellulosic solid residues (CSR), were mechanically fibrillated at 1 wt% concentration using a microfluidizer (Microfluidizer M-110EH, Microfluidics Corp., Westwood, MA) to produce CNFs (Wang et al. 2012, 2013). The CSR suspension was processed for either 5 or 10 passes through a 200 μm chamber and an 87 μm chamber in a series at 80 MPa. After microfluidization, the CSR suspension became gel, indicating that the CSR has been fibrillated into nano dimensions.

Table 1 Lists of chemical compositions and DP of the feeding cellulosic materials and hydrolyzed WIS under different conditions, along with properties of CNCs and the yields of CNCs and CSRs

| Sample label | Chemical composition | | | Yields[a] | | | | Hydrolyzed WIS DP | Properties of CNCs | | | | CrI (%) | | T_{95} (°C) | T_{onset} (°C) |
	Glucan (%)	Xylan (%)	Mannan (%)	Sugar (%)	CNCs (%)	CSR (%)	Total (%)		Particle Size (nm)	Polydispersity index	Zeta potential (mV)	COOH (mmol/g CNCs)	XRD	Raman		
BEP	76.1 ± 0.4	15.6 ± 0.2	ND					1001 ± 44					77.3	59.7	322	309
BEP-O10	80.8 ± 0.3	13.8 ± 0.2	ND	4.05	0	92.03	96.08	395 ± 2								
BEP-O30	82.7 ± 2.0	12.2 ± 0.4	ND	6.14	2.60	86.06	94.80	276 ± 2	239 ± 9	0.28 ± 0.02	−36.6 ± 1.0	0.150	76.0	50.9	261	262
BEP-O50	81.5 ± 0.1	10.6 ± 0.1	ND	8.78	4.39	82.70	95.87	239 ± 2	205 ± 3	0.24 ± 0.06	−44.3 ± 1.2	0.199	76.1	52.8	315	307
SDP	87.3 ± 1.1	4.3 ± 0.6	4.8 ± 0.6					1233 ± 21					NA	NA	326	327
SDP-O10	91.6 ± 1.3	3.1 ± 0.1	4.9 ± 0.1	2.04	0	96.11	98.15	165 ± 2								
SDP-O30	90.4 ± 1.6	2.6 ± 0.1	3.7 ± 0.1	2.99	2.25	91.46	96.70	121 ± 1	346 ± 11	0.31 ± 0.03	−42.4 ± 2.8	0.316	NA	NA	282	272
SDP-O50	90.1 ± 1.5	1.9 ± 0.1	3.5 ± 0.7	7.88	5.04	82.82	95.74	112 ± 0	174 ± 1	0.27 ± 0.01	−48.1 ± 2.0	0.240	NA	NA	279	282
QFP	82.6 ± 2.2	8.1 ± 0.1	7.0 ± 0.4					1115 ± 26					80.5	63.4	327	334
QFP-O10	82.1 ± 0.5	6.9 ± 0.2	6.7 ± 1.7	1.65	0	94.50	96.15	341 ± 2								
QFP-O30	82.1 ± 2.4	7.6 ± 1.0	8.4 ± 0.2	3.07	3.02	89.81	95.90	256 ± 1	284 ± 3	0.27 ± 0.02	−33.8 ± 1.0	0.067	79.1	53.7	301	320
QFP-O50	86.1 ± 2.5	8.1 ± 0.2	7.6 ± 0.5	6.03	5.81	83.67	95.51	220 ± 5	247 ± 1	0.24 ± 0.02	−45.3 ± 2.3	0.072	80.6	60.2	318	316

ND not detected, *NA* not applicable

[a] The data represent the weight percentage based on the OD weight of starting materials and CSR
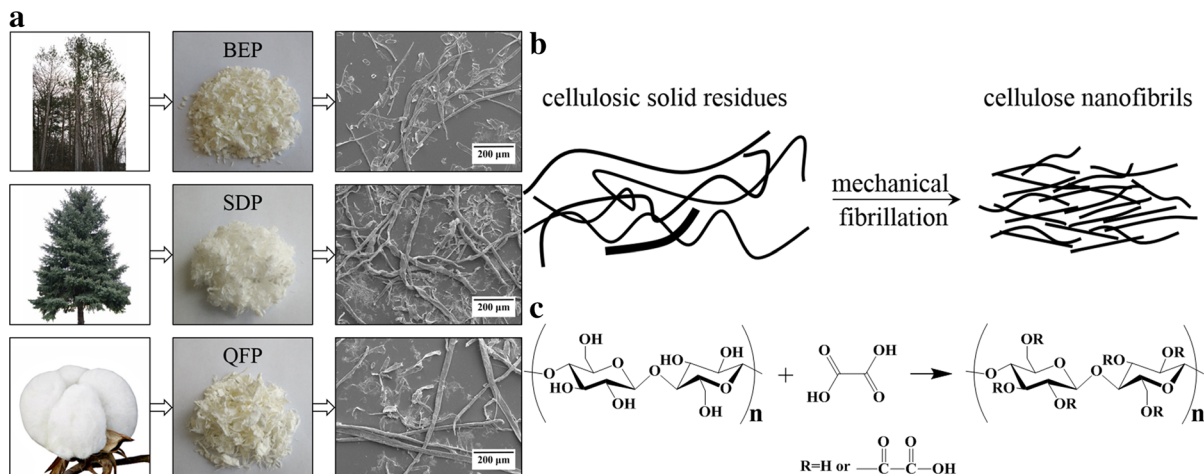
Fig. 1 **a** Cellulosic materials and their SEM images. **b** Schematic diagram of CNFs preparation. **c** Reaction scheme illustrating cellulose esterification of hydroxyl groups

The CNF gels were stored in a cold room (4 °C) for further tests.

To facilitate discussion, the CNC and CNF samples are labelled as xxx-Oyy and xxx-OyyPz in an abbreviated form, respectively, where xxx stands for the starting materials (BEP, SDP and QFP), yy stands for oxalic acid concentration (10, 30, or 50 wt%), and z stands for the number of passes in microfluidization (5 or 10).

Determination of CNC yield

The volume of the separated CNC suspensions was recorded. CNCs yields were determined by a chemical oxygen demand (COD) method described previously (Wang et al. 2012).

Degree of polymerization

The DP of the starting materials, hydrolyzed washed water insoluble solids (WIS), and CNFs were determined according to the ES ISO 5351:2012 Standard. Vacuum dried cellulosic solids of 0.1 g was first dispersed in 10 mL DI water, then added 10 mL of 1 M cupriethylenediamine solution. The viscosity of the resultant solution was measured in a capillary viscometer at 25 °C. The intrinsic viscosity [η] of each solution was determined according to the standard. The DP value of the cellulose was calculated according to the following equation (Sihtola et al. 1963).

$$DP^{0.905} = 0.75[\eta]$$

Duplicate measurements were conducted and the averages were reported.

SEM and AFM imaging

The cellulosic materials and CSRs were examined using a Zeiss EVO 40 SEM system (Carl Zeiss NTS, Peabody, MA). All the samples were sputter-coated with gold to provide adequate conductivity.

The morphologies of CNCs and CNFs were observed by AFM imaging. Suspensions of approximately 0.01 wt% CNCs or CNFs were dispersed under sonication and deposited on a mica substrate, then air dried at ambient temperature. The CNCs and CNFs were imaged in vibrating tapping mode on an AFM system (CS-3230, AFMWorkshop, CA, USA). The diameter and length distributions of CNCs and CNFs were obtained by analyzing the AFM images of at least 83 individual CNC or CNF using Image-Pro Plus software (Media Cybernetics, Silver Spring, USA).

Particle size distribution and zeta potential

The particle size distribution and zeta potential of all the CNC and CNF suspensions were analyzed by a NanoBrook Omni Particle Size and Zeta Potential Analyzer (Brookhaven Instruments, Holtsville, NY, USA) based on dynamic light scattering (DLS) and phase analysis light scattering (PALS). All the sample

suspensions were ultrasonically treated (QSONICA, 3510R-MT, 42 kHz and 100 W, Newtown, CT, USA) for 10 min before analysis, and the concentration of all samples was 0.2 g/L. For each sample, the measurements of zeta potential were conducted for 5 times and 20 cycles. The measurements of particle size were repeated five times and the average results were reported.

Esterification and carboxylation determination

Cellulose esterification by oxalic acid was identified by a Fourier transform infrared (FTIR) spectroscopy system (Spectrum Two, PerkinElmer, Waltham, MA) equipped with a universal attenuated-total-reflection (ATR) probe in a range of 450–4000 cm^{-1} with a resolution of 4 cm^{-1}. Each sample was scanned 4 times. The carboxyl group content of CNCs was determined by conductometric titration as described previously (Bian et al. 2017b; Chen et al. 2016).

Light transmittance

The UV–Vis light transmittance spectra of CNC and CNF suspensions (0.1 wt%) were measured in a wavelength range of 190–1100 nm using a spectrophotometer (Model 8453, Agilent Technologies, Inc., USA).

X-ray diffraction (XRD) analysis

X-ray diffraction patterns of the cellulosic materials and the CNC samples were determined using a X-ray diffractometer (Bruker D8 Discover, Bruker Co., Billerica, MA) equipped with Cu Kα radiation in the 2θ range of 10°–38° in steps of 0.02°. The crystallinity index (CrI) of BEP, QFP and their corresponding CNCs was calculated according to the empirical method developed by Segal et al. (1959):

$$CrI = \frac{I_{200} - I_{am}}{I_{200}} \times 100\%$$

where I_{200} is the maximum peak intensity at (200) lattice diffraction and I_{am} is the minimum diffraction intensity between planar reflections (110) and (200).

FT-Raman

FT-Raman spectra of cellulose materials and the corresponding CNC samples were measured by a Bruker MultiRam spectrometer (Bruker Instruments Inc., Billerica, MA) equipped with a 1064 nm 1000 mW continuous wave, diode-pumped Nd:YAG laser in the wavenumber range of 50–3700 cm^{-1} with 1024 scans at a resolution of 4 cm^{-1}. The laser power used for sample excitation was 660 mW and Bruker's OPUS software program was used for spectral processing. Spectra were compared after normalizing at 1096 cm^{-1} and peak heights (PH) of specific bands were calculated as relative to the peak height at 1096 cm^{-1}. Instrument software OPUS was used to calculate such data. Crystallinities by Raman were estimated using the 380-Raman method (Agarwal et al. 2010, 2013) according to the following equations.

$$X_{MultiRam} = ((I_{380}/I_{1096}) - 0.0286)/0.0065 \quad (1)$$

$$X_{RFS-100} = (X_{MultiRam} + 2.0212)/0.8222 \quad (2)$$

Thermogravimetric analysis (TGA)

The thermal stability of cellulosic materials and the resultant CNCs was measured using a thermogravimetric analyzer (Pyris 1 TGA, PerkinElmer Inc., Waltham, MA). The samples were heated in the temperature range from 50 to 600 °C at a heating rate of 10 °C/min under a nitrogen atmosphere with a flow rate of 20 mL/min. All the samples were dried at 50 °C for 4 h before testing to remove the moisture.

Results and discussion

CNC yields

CNC yields were low (Table 1) due to the weak strength of oxalic acid at low acid concentrations (≤50 wt%), agree with previous studies (Chen et al. 2016; Wang et al. 2017). The CNC yield was increased with acid concentration, but not much affected by the different starting materials used. The maximal CNC yield was approximately 5% at acid concentration of 50 wt%. Cellulose loss to glucose was minimal (Table 1 based on glucan content in CSR and CSR and CNC yields) and slightly increased with acid concentration for SDP. Overall, acid hydrolysis decreased hemicellulose content in CSR due to dissolution to sugars. Total sugar yields were less than 10% with mostly from dissolved hemicelluloses.
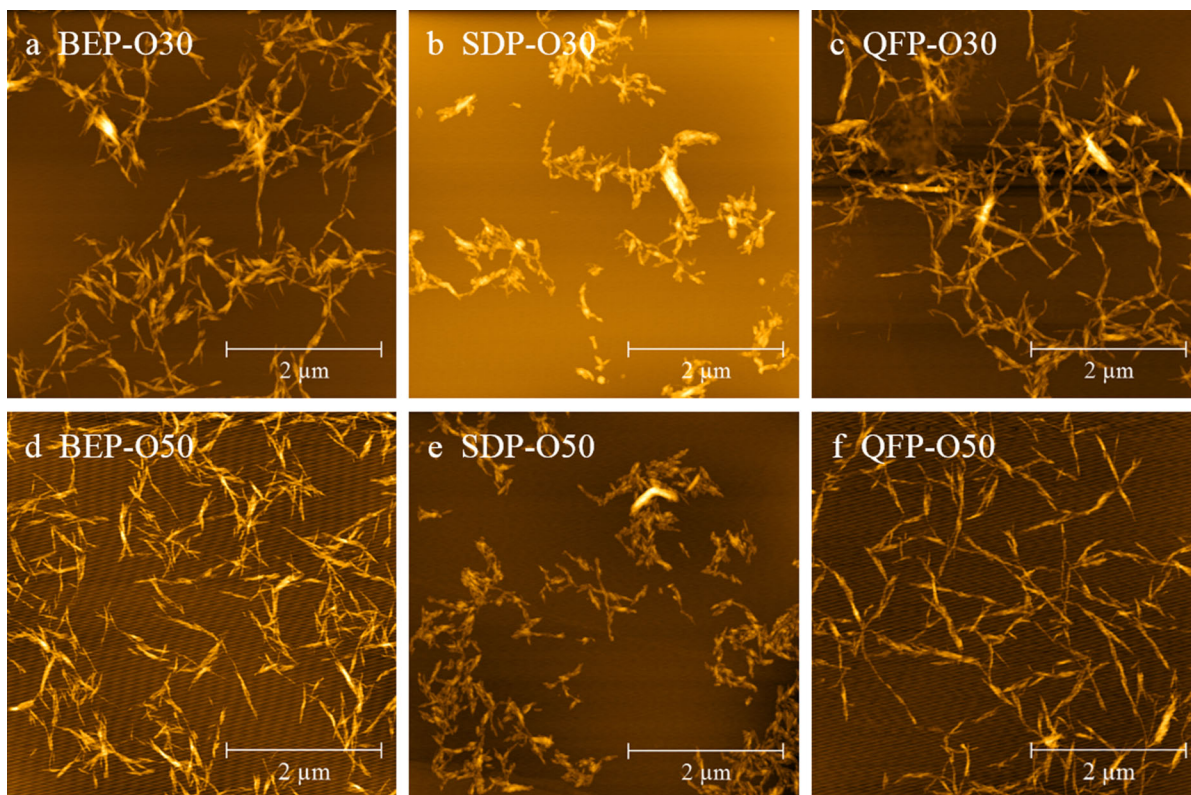
Fig. 2 AFM topographic images of CNCs prepared using different starting materials at different oxalic acid concentrations. *Scale* = 2 μm

Most of the feed fibers were remained as CSR after hydrolysis with yield over 80% that can be used for CNF production through subsequent mechanical fibrillation.

Morphologies

Acid hydrolysis mainly cut fibers through depolymerization of cellulose as revealed by the DP of the hydrolysis products (Table 1) and SEM imaging (Fig. S1) especially at acid concentration >30 wt%. It seems acid hydrolysis also solubilized fines (short microfibers) based on SEM images, in agreement with previous studies using enzymatic hydrolysis (Wang et al. 2015; Zhu et al. 2011).

AFM images clearly revealed the morphological differences among CNCs from different feed fibers (Fig. 2). Aggregates were visible at acid concentration of 30 wt% (Fig. 2a–c) especially for SDP-O30 (Fig. 2b). Aggregates remained visible from the SDP CNC sample produced at 50 wt% acid concentration

(Fig. 2e) and may have something to do with its different polymorphic nature (cellulose II), but not the CNC samples from BEP (Fig. 2d) and QFP (Fig. 2f). The CNCs from SDP are much shorter of approximately 100–200 nm than those from BEP and QFP. Crystal length as long as 2000 nm were apparent for CNCs from QFP (cotton) (Fig. 2f) while typical crystal length of approximately 500 nm for CNCs from BEP (Fig. 2d).

Previous research using sulfuric acid, a strong mineral acid, showed that the size of CNC is strongly dependent on the hydrolysis conditions especially acid concentrations (Chen et al. 2015). This is also revealed qualitatively in this study as shown by AFM (Fig. 2). Quantitative analyses of the AFM images indicated that CNCs obtained using oxalic acid concentration of 50 wt% had a more finer dimension, 36, 38, and 37 nm, for BEP, SDP, and QFP, respectively, compared with 39, 51, and 44 nm for CNCs obtained at a low concentration of 30 wt% from the same feed fibers (Fig. S3). CNCs lengths were also quantitatively
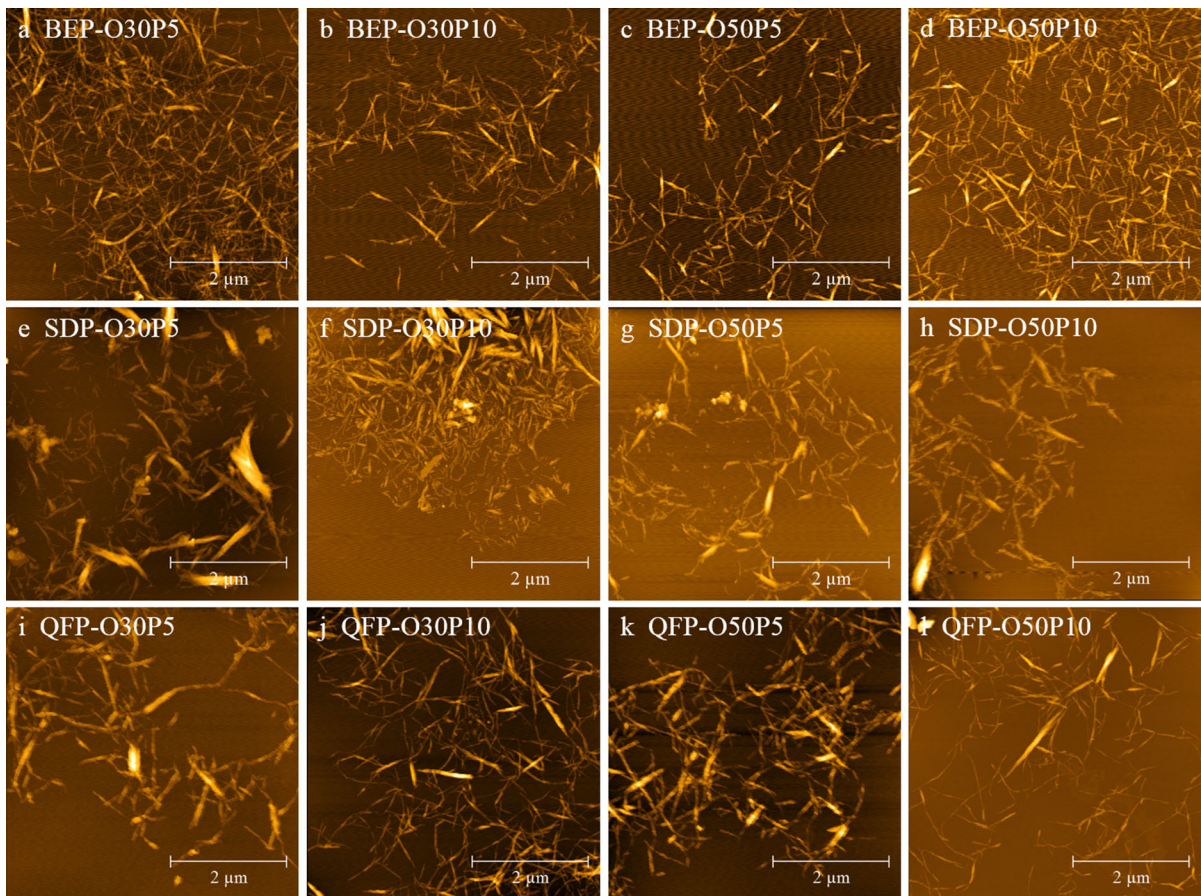
Fig. 3 AFM topographic images of CNFs prepared using different starting materials at different oxalic acid concentrations and different number of passes through microfluidization. *Scale* = 2 μm

measured from AFM images as both ends of a CNC crystal can be easily identified when a CNC suspension is well dispersed as shown in Fig. 2. The average lengths of CNCs obtained at oxalic acid concentration of 50 wt% from BEP, SDP and QFP were 515, 203 and 670 nm, respectively. Based on AFM measured mean lengths and diameters, the average aspect ratios of the three CNCs were 14, 5, and 18, respectively. The true aspect ratio may well be greater than the reported values due to the fact that AFM tip broadening is more pronounced in the diameter dimension than in the length dimension (Deepa et al. 2015).

Different morphologies were also observed among different CNF samples from three different starting fibers. It appears that acid concentration and the number of passes through microfluidization did not substantially affect the morphology of the BEP-CNF

samples (Fig. 3a–d). Perhaps due to sufficient acid hydrolysis that resulted in similar CSR DP (Table 1) and the low pressure of the microfluidization process compared with that used in a previous study (Chen et al. 2016). Higher acid concentration and more passes through microfluidization apparently produced less aggregated and finer fibrils from SDP and QFP fibers (Fig. 3e–l). Quantitative CNF length measurements were not performed due to fibril entanglement. It is estimated, however, from AFM images that typical fibril length is approximately 1000 nm, which resulted in an estimated aspect ratio of approximately 30, greater than those of CNC samples. Fibril aspect ratio is an important parameter for composites to improve mechanical properties. The higher the aspect ratio of the CNFs, the better the mechanical properties of the composite (Moon et al. 2011).

The particle size was also analyzed by dynamic light scattering (DLS). Although DLS cannot provide accurate measurements for rod-like particles, it can produce qualitative numeric results very quickly. It has been used for CNC characterization by several studies (Li et al. 2015; Yu et al. 2013). The DLS particle size and polydispersity index of CNC samples are given in Table 1. Since DLS measures the diffusion coefficient of the particles which is then converted into a hydrodynamic radius by the Stokes–Einstein equation, the size given by this technique is the radius of a sphere that has the same diffusion coefficient as a rod-like CNC particle. Results, in the case of nanorods, can therefore only be considered as an indication of the possible presence of aggregates and as an evaluation of the size polydispersity (Brito et al. 2012). DLS data undoubtedly showed that CNC sizes are clearly dependent on the concentration of oxalic acid used in acid hydrolysis. The CNC sample produced at a higher oxalic acid concentration had a smaller DLS particle size, i.e., the DLS size of CNCs decreased from 239, 346 and 284 nm to 205, 174 and 247 nm, for BEP, SDP, and QFP CNCs respectively, when the acid concentration was increased from 30 to 50 wt%. In addition, the CNCs prepared at a higher acid concentration had a smaller polydispersity index, i.e., a more uniform size was generated. All these results are in agreement with AFM imaging results.

Degree of polymerization

The effects of oxalic acid concentration and the number of passes through microfluidization on the DP of different cellulose materials are reported in Tables 1 and S1. The hydrolyzed washed WIS DP values of BEP, SDP and QFP were substantially reduced from their starting materials of 1001, 1233 and 1115, respectively, by acid hydrolysis. Even at 10% oxalic acid concentration, SDP already reached level off DP (LODP) of 165 after 1 h hydrolysis at 100 °C. DP were reduced to 395 and 341 for BEP and QFP, respectively. DP reduction is slow with further increase in acid concentration, in agreement with our previous study (Wang et al. 2017). SDP has a higher DP of 1233 than the BEP of 1001. The hydrolyzed BEP samples, however, had much greater DP values than those of hydrolyzed SDP samples. It can be observed from Table S1 that increasing the pass number of microfluidization did not reduce the DP of

cellulose perhaps due to the fact that LODP was reached.

Esterification, carboxylation, and surface charge

FTIR spectra of the CNC samples show the typical absorption bands of cellulosic materials (Fig. 4a–c). A strong absorption band at about 3332 cm^{-1} is related to the stretching vibration of hydroxyl groups (–OH), and the absorption band at about 2896 cm^{-1} results from the symmetric C–H stretching vibration (Liu et al. 2014). The peaks at around 1640 and 1024 cm^{-1} can be attributed to O–H bending vibration of the
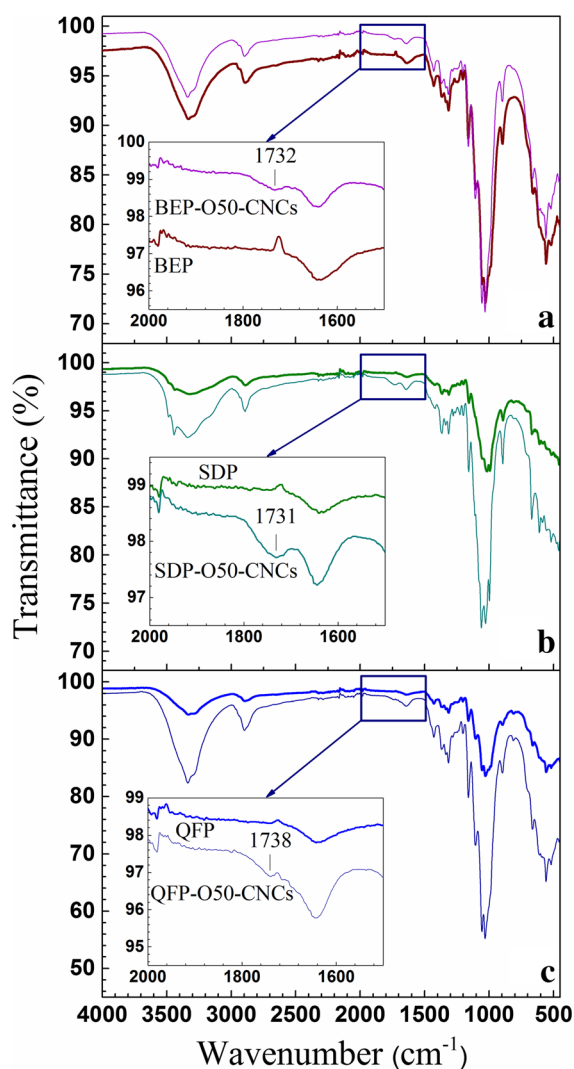

Fig. 4 Comparisons of FTIR spectra between the CNC samples and their corresponding feed fibers

Table 2 Selected IR and Raman spectral data of cellulose materials and the corresponding CNCs

Sample label	IR (cm^{-1})	Raman (cm^{-1})								
	~ 1732	128	352	380	577	637	802	1602	1750	3064
BEP	ND	X, w	X, w	X	ND	ND	ND	ND	ND	ND
BEP-O30	X	ND	X, w	X	ND	X	X	X	X, w	X
BEP-O50	X	ND	X, w	X	ND	X	X	X	X	X
SDP	ND	X, w	X	X, wr	X	ND	ND	ND	ND	ND
SDP-O30	X	X, sr	X	X, wr	X, sr	ND	ND	X	X, w	ND
SDP-O50	X	X, sr	X	X, wr	X, sr	ND	ND	X, w	X	ND
QFP	ND	ND	X, w	X	ND	ND	ND	ND	ND	ND
QFP-O30	X	ND	X, w	X	ND	ND	ND	X, w	ND	ND
QFP-O50	X	ND	X, w	X	ND	ND	ND	X, w	ND	ND

ND not detected, *X* detected, *w* weak, *wr* weaker, *sr* stronger

absorbed water (Eyholzer et al. 2010; Lu and Hsieh 2010) and C–O–C stretching vibration of pyranose ring (Deepa et al. 2015), respectively. The peak at 893 cm^{-1} can be assigned to β-glycosidic linkages of glucose ring in cellulose (Ganan et al. 2004). When comparing the CNC FTIR spectrum with its corresponding feed fibers, a new peak appeared at approximately 1732, 1731, and 1738 cm^{-1} for CNCs from BEP, SDP and QFP, respectively (Table 2), corresponding to the C $=$ O ester vibrational stretching band (Spinella et al. 2015). This confirms the esterification of cellulose by oxalic acid. The ester and carboxylic C=O stretch bands at 1602 and 1750 cm^{-1}, respectively were also detected in the Raman spectra of some of the samples (Table 2) which further supported this observation. The peaks in IR and Raman are not very strong for all the CNC samples, suggesting that the carboxylation and esterification degree is moderate (Bian et al. 2017a; Chen et al. 2016; Wang et al. 2017). In Raman, only for BEP CNCs additional peaks were detected at 637, 802, and 3064 cm^{-1} (Table 2; Fig. S6). However, presently, it is not clear what these peaks represent but it is important to note that these contributions were absent in the two other types of CNCs.

It is hypothesized that only one carboxyl group in oxalic acid esterified cellulose, which leaves the other carboxyl group on CNC surface to result in charged CNCs. This is supported by the Raman data (Table 2) where in the spectra of all the CNCs a band with varying intensity at 1602 cm^{-1} was present (Fig. S6). None of the Raman spectra of the starting materials had a contribution at this wavenumber. Additionally, conductometric titration of the CNC samples

confirmed the existence of carboxyl groups (Table 1). Furthermore, the carboxyl group content increased with acid concentration. Zeta potential measurements confirmed that the CNC samples are highly negatively charged. Moreover, the zeta potentials were in general positively correlated to the carboxyl group contents, suggesting CNC surface charge was primarily contributed by the carboxyl groups. The CNF samples also carry quite highly negative charge (Table S1) though not as high as their corresponding CNC samples, suggesting CNFs were also carboxylated and had lower carboxyl group contents compared to corresponding CNC samples.

Properties of CNC and CNF suspensions

Transmittance of CNC suspensions at 0.1% consistency was measured. QFP-O50 has the highest transmittance of 68% at 600 nm as shown in Fig. 5a, b. The transmittance of the CNC suspensions from BEP were substantially affected by acid concentration in hydrolysis, i.e., increased from 8 to 56% at 600 nm when acid concentration was increased from 30 wt% (BEP-O30) to 50 wt% (BEP-O50). On the other hand, the transmittance of the CNC suspensions from SDP were lower even at acid concentration of 50 wt% (SDP-O50).

The ability of the CNF samples to form stable suspensions or gels in water at very low concentration of 0.1% was evaluated by qualitatively analyzing the aggregation and sedimentation behaviors of the suspensions. Photographs of the three aqueous suspensions were taken after 0, 24, and 48 h of ultrasonication (Fig. 5c). The CNF suspensions prepared from BEP and QFP aggregated quickly after
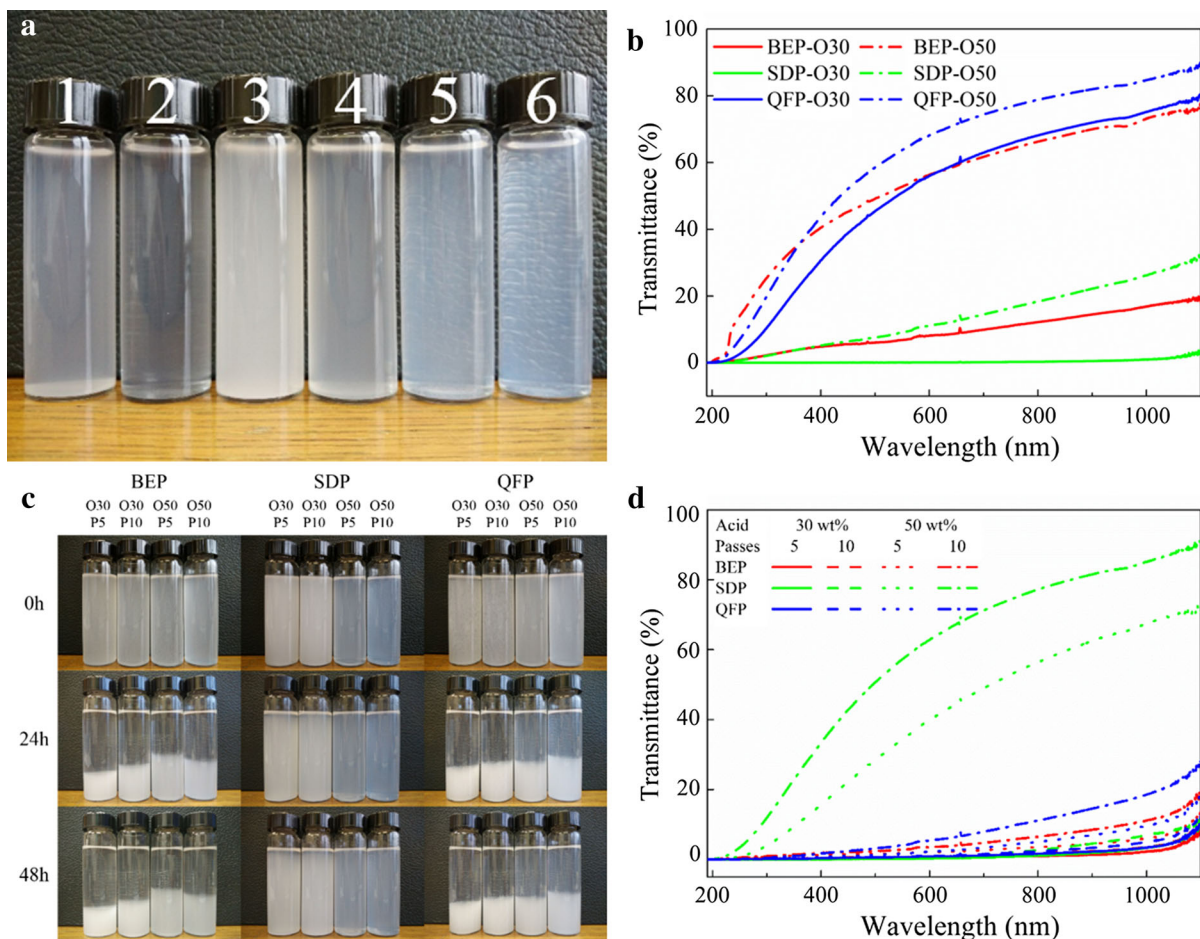
Fig. 5 **a** Images of CNC suspensions, *1* BEP-O30, *2* BEP-O50, *3* SDP-O30, *4* SDP-O50, *5* QFP-O30, *6* QFP-O50. **b** UV–Vis light transmittance spectra of CNC suspensions. **c** Aggregation and sedimentation behaviors of CNF suspensions. Pictures were taken at 0, 24, and 48 h, respectively after ultrasonication. **d** UV–Vis light transmittance spectra of CNF suspensions. All the CNC and CNF suspensions concentrations were 0.1 wt%

ultrasonication despite the fact that they have high surface charge compared to the corresponding CNF samples from SDP (Table S1). With prolonged time, lots of sedimentations were appeared at the bottom of the bottles. Complete sedimentation of the CNF suspensions of BEP and QFP occurred within 24 h. In contrast, the CNFs from SDP could be well dispersed in water to form homogeneously dispersed suspensions and no obvious sedimentation could be observed. The good stability was maintained even after 48 h. Indeed, it was difficult to distinguish the sedimentation behaviors among different SDP CNF suspensions. However, the transparency of the CNF suspensions varied tremendously. The samples (SDP-O30P5 and SDP-O30P10) obtained by 30 wt% oxalic acid hydrolysis formed opaque suspensions, whereas

the samples (SDP-O50P5 and SDP-O50P10) obtained by 50 wt% oxalic acid hydrolysis were translucent. Their transmittance at 600 nm are 40 and 63%, respectively, as shown in Fig. 5d. The high light transmittance is caused by the stable dispersion. The transmittances of other CNF suspensions varied little and is low, which can be ascribed to the poor dispersibility. In addition, the transparency of SDP-O50 indicates that the dimensions of a major part of cellulose particles in the suspensions are below the limit of light-scattering.

The stability of the CNF suspensions is expected to depend on the size and the surface characteristics of the CNFs. The particle sizes and zeta potentials of the CNFs are listed in Table S1. Many researches have shown that the larger the absolute value of zeta

potential is, the better suspension stability that can be achieved due to electrostatic repulsion between the nanoscale particles (Liu et al. 2014). For the CNFs obtained from BEP, though they have relatively higher zeta potentials (absolute value, the same below) compared with the SDP CNFs, their sizes are also greater, to result in poor dispersion. For the CNFs obtained from QFP, they had both great particle size and low zeta potential at the same time, to result in poor stability. As for the CNFs from SDP, although their zeta potentials were not very high, but they had small particle size, especially for SDP-O50P5 and SDP-O50P10, their sizes can be comparable to those of CNCs obtained from SDP, thus resulting in good dispersion. SDP CNFs are mostly cellulose II polymorphs, which may also contribute to good dispersion as cellulose II has better interaction with water than cellulose I polymorph (Agarwal et al. 2016). Both Raman and XRD provided the evidence for the existence of cellulose II polymorphs in the SDP samples. In Raman, cellulose II was detected based on appearance of a band at 577 cm^{-1} (Agarwal 2014) (Table 2; Fig. S6). On the other hand, in XRD, the presence of significant amount of cellulose II is seen from its [110] reflection plane peak (see below).

Crystallinity of CNCs

XRD measurements indicated that BEP and QFP as well as their corresponding CNCs have three characteristic peaks at about 16.4°, 22.6° and 34.5°, corresponding to the (110), (200), and (004) reflection planes of typical cellulose I structure, respectively (Lin and Dufresne 2014). For the patterns of SDP and its corresponding CNCs, there are four major diffraction peaks, which are located at around 12.1°, 20.1°, 21.9° and 34.7°, and assign to the (1$\bar{1}$0), (110), (020), and (004) crystallographic planes of typical cellulose II structure, respectively (Lu et al. 2015; Mansikkamaki et al. 2005). The diffraction patterns of CNCs are not significantly different from that of cellulose materials, revealing that oxalic acid hydrolysis did not destroy or alter the inherent crystal structures of cellulose. This was also supported by the Raman spectra of the starting materials and the corresponding CNCs (Fig. S6). The values of the CrI were estimated from both XRD and Raman and are summarized in Table 1. In XRD,
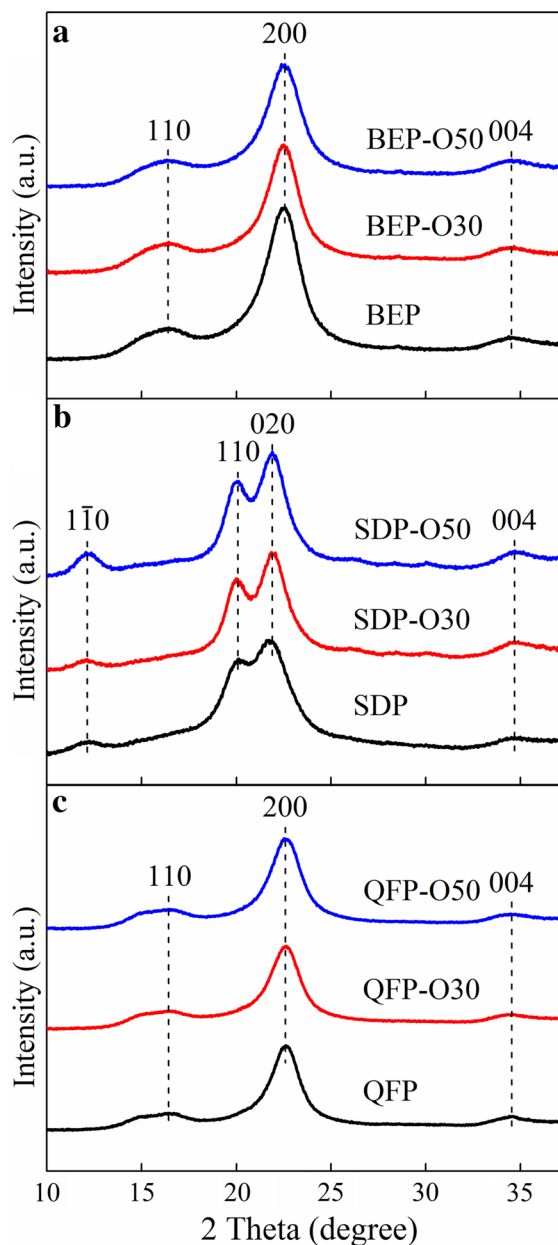

Fig. 6 XRD patterns of cellulose materials and their corresponding CNCs

the CrI of BEP, QFP and their corresponding CNCs were calculated using the diffractogram patterns. In Raman, except for the CrIs of SDP and the corresponding CNCs, those of the other materials were obtained from their Raman spectra (Fig. S6). Equation 2 earlier in the FT-Raman section was used to calculate CrIs. The Raman method is based on the
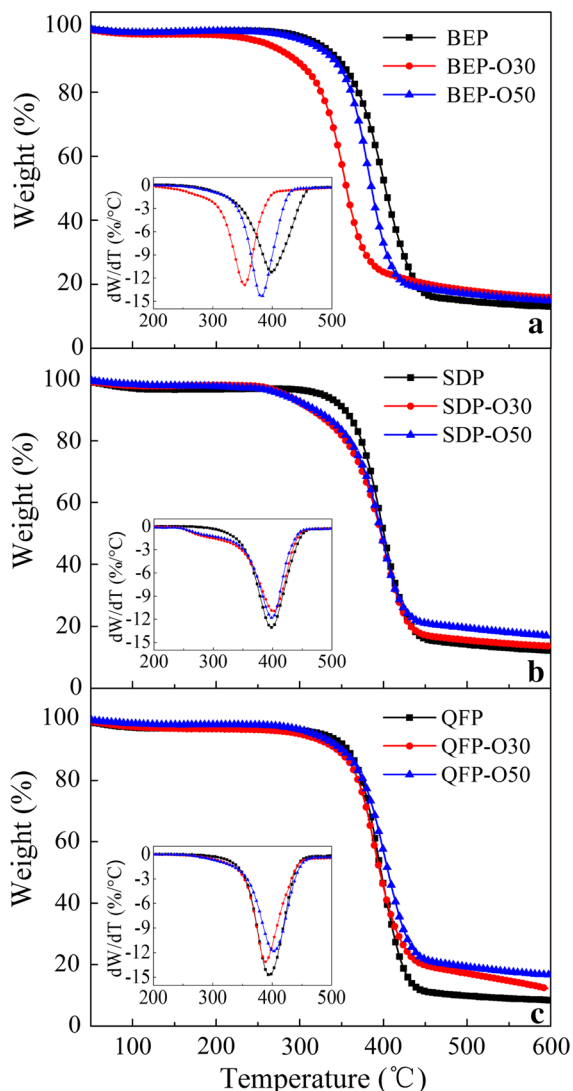
Fig. 7 TG and DTG curves of cellulose materials and the corresponding CNCs

(380/1096) peak height ratio. Further details can be found elsewhere (Agarwal et al. 2010, 2013). The calculated XRD CrIs of BEP and QFP starting materials are 77.3 and 80.5%, respectively (Table 1). Compared with the CrIs of BEP and QFP, no obvious change is observed for the CNCs made from them. On the other hand, Raman CrIs data indicated that the crystallinity declined slightly when CNCs were produced from BEP and QFP (from 59.7 to 50.9 and 52.8%, respectively, for BEP-O30 and BEP-O50 CNCs; from 63.4 to 53.7 and 60.2%, respectively, for QFP-O30 and QFP-O50 CNCs). However, CrIs for

the SDP could not be calculated due to the presence of high amount of cellulose II in these samples (based on 577 cm^{-1} band in Raman, cellulose II was present at 69.7, 81.8, and 97.2% in SDP, SDP-O30, and SDP-O50, respectively). The presence of higher amount of cellulose II in the SDP CNCs caused the Raman bands at 1280 cm^{-1} to become more intense (Fig. 6). Although not proven yet, the latter may also have to do with higher cellulose II crystallinity of the CNCs (Agarwal 2014).

Thermal stability of CNCs

TG and DTG curves of the three cellulose materials and their corresponding CNCs are compared (Fig. 7). The temperature at 5% weight loss (T_{95}) and the onset decomposition temperature (T_{onset}) were determined (Table 1). Here the T_{onset} was defined at $dW/dT \geq -1$, i.e., at which weight loss is greater or equal to 1% with an increase in temperature of 1 °C (Chen et al. 2016). The thermal decomposition of cellulose involves depolymerization, dehydration, and decomposition of glycosidic units followed by the formation of a char residue (Yu et al. 2013). The T_{onset} of BEP, SDP and QFP starting materials are 309, 327 and 334 °C, respectively. All CNC samples exhibited lower thermal stability compared with the starting materials, the high surface area of CNCs plays an important role in reducing their thermal stability because of the increased exposure surface area to heat (Lu and Hsieh 2010). The existence of carboxyl groups on the surface of CNCs may also contribute to low thermal stability as found in TEMPO-mediated oxidized CNCs and ammonium persulfate oxidized CNCs (Zhang et al. 2016a). Interestingly, however, T_{onset} of CNCs BEP-O50 (=307 °C) obtained at 50 wt% oxalic acid concentration has a higher carboxyl group content is higher than BEP-O30 [=262 > 218 °C of BEP CNCs from sulfuric acid hydrolysis (Chen et al. 2016)] as listed in Table 1. Furthermore, our previous study (Chen et al. 2016) indicated that BEP CNCs produced at 70 wt% oxalic acid concentration had an even higher $T_{onset} = 322$ °C despite with highest carboxyl group content among the three samples. These results suggest that carboxyl group content is not a major adverse contributing factor to thermal stability. Similar trends were also observed in CNCs produced from SDP. The acid concentration had negligible effect on thermal stability of CNCs from QFP.

Conclusions

CNCs and CNFs were successfully produced by hydrolysis using oxalic acid at different concentrations and subsequent mechanical fibrillation from bleached eucalyptus pulp, spruce dissolving pulp and cotton based qualitative filter paper. The DP values of cellulose materials decreased substantially after hydrolysis, whereas the mechanical fibrillation did not dramatically reduce the DP of cellulose. CNFs derived from SDP presented the best suspension stability. The CNCs and CNFs obtained from BEP and QFP possessed more uniform dimensions. CNCs with different aspect ratios could be produced from different starting materials by oxalic acid hydrolysis. FTIR and Raman spectroscopies demonstrated that carboxylated CNCs were obtained from a variety of starting materials by oxalic acid hydrolysis. The results of XRD and FT-Raman analyses indicated that, depending on the method of analysis, the crystallinity of CNCs from BEP and QFP either had no change compared with their starting materials or declined only slightly (<10%). CNCs obtained from QFP exhibited higher thermal stability compared to those obtained from BEP and SDP, and all the CNCs possessed better thermal stability than that of CNCs from sulfuric acid hydrolysis, which are important for a range of advanced applications.

References

Agarwal UP (2014) 1064 nm FT-Raman spectroscopy for investigations of plant cell walls and other biomass materials. Front Plant Sci 5(490):1–12

Agarwal UP, Reiner RS, Ralph SA (2010) Cellulose I crystallinity determination using FT-Raman spectroscopy: univariate and multivariate methods. Cellulose 17(4):721–733

Agarwal UP, Reiner RR, Ralph SA (2013) Estimation of cellulose crystallinity of lignocelluloses using near-IR FT-Raman spectroscopy and comparison of the Raman and Segal-WAXS methods. J Agric Food Chem 61(1):103–113

Agarwal UP, Ralph SA, Reiner RS, Baez C (2016) Probing crystallinity of never-dried wood cellulose with Raman spectroscopy. Cellulose 23(1):125–144

Beltramino F, Blanca Roncero M, Vidal T, Torres AL, Valls C (2015) Increasing yield of nanocrystalline cellulose preparation process by a cellulase pretreatment. Bioresour Technol 192:574–581

Bian H, Chen L, Dai H, Zhu JY (2017a) Integrated production of lignin containing cellulose nanocrystals (LCNC) and nanofibrils (LCNF) using an easily recyclable di-carboxylic acid. Carbohyd Polym 167:167–176

Bian H, Chen L, Wang R, Zhu JY (2017b) Green and low-cost production of thermally stable and carboxylated cellulose nanocrystals and nanofibrils using highly recyclable dicarboxylic acids. J Vis Exp. doi:10.3791/55079

Biyani MV, Foster EJ, Weder C (2013) Light-healable supramolecular nanocomposites based on modified cellulose nanocrystals. Acs Macro Lett 2(3):236–240

Bondeson D, Mathew A, Oksman K (2006) Optimization of the isolation of manocrystals from microcrystalline cellulose by acid hydrolysis. Cellulose 13:171–180

Braun B, Dorgan JR (2009) Single-step method for the isolation and surface functionalization of cellulosic nanowhiskers. Biomacromolecules 10(2):334–341

Brito BSL, Pereira FV, Putaux J-L, Jean B (2012) Preparation, morphology and structure of cellulose nanocrystals from bamboo fibers. Cellulose 19(5):1527–1536

Chen L, Wang Q, Hirth K, Baez C, Agarwal UP, Zhu JY (2015) Tailoring the yield and characteristics of wood cellulose nanocrystals (CNC) using concentrated acid hydrolysis. Cellulose 22(3):1753–1762

Chen L, Zhu JY, Baez C, Kitin P, Elder T (2016) Highly thermal-stable and functional cellulose nanocrystals and nanofibrils produced using fully recyclable organic acids. Green Chem 18:3835–3843

Cirtiu CM, Dunlop-Briere AF, Moores A (2011) Cellulose nanocrystallites as an efficient support for nanoparticles of palladium: application for catalytic hydrogenation and Heck coupling under mild conditions. Green Chem 13(2):288–291

de Castro DO, Bras J, Gandini A, Belgacem N (2016) Surface grafting of cellulose nanocrystals with natural antimicrobial rosin mixture using a green process. Carbohyd Polym 137:1–8

Deepa B, Abraham E, Cordeiro N, Mozetic M, Mathew AP, Oksman K, Faria M, Thomas S, Pothan LA (2015) Utilization of various lignocellulosic biomass for the production of nanocellulose: a comparative study. Cellulose 22(2):1075–1090

Dong XM, Revol JF, Gray DG (1998) Effect of microcrystallite preparation conditions on the formation of colloid crystals of cellulose. Cellulose 5(1):19–32

Eichhorn SJ, Dufresne A, Aranguren M, Marcovich NE, Capadona JR, Rowan SJ, Weder C, Thielemans W, Roman M, Renneckar S et al (2010) Review: current international research into cellulose nanofibres and nanocomposites. J Mater Sci 45(1):1–33

Espinosa SC, Kuhnt T, Foster EJ, Weder C (2013) Isolation of thermally stable cellulose nanocrystals by phosphoric acid hydrolysis. Biomacromolecules 14(4):1223–1230

Eyholzer C, Bordeanu N, Lopez-Suevos F, Rentsch D, Zimmermann T, Oksman K (2010) Preparation and characterization of water-redispersible nanofibrillated cellulose in powder form. Cellulose 17(1):19–30

Filson PB, Dawson-Andoh BE (2009) Sono-chemical preparation of cellulose nanocrystals from lignocellulose derived materials. Bioresour Technol 100(7):2259–2264

Ganan P, Cruz J, Garbizu S, Arbelaiz A, Mondragon M (2004) Stem and bunch banana fibers from cultivation wastes: effect of treatments on physico-chemical behavior. J Appl Polym Sci 94(4):1489–1495

Guru M, Bilgesu AY, Pamuk V (2001) Production of oxalic acid from sugar beet molasses by formed nitrogen oxides. Bioresour Technol 77(1):81–86

Hamad WY, Hu TQ (2010) Structure–process–yield interrelations in nanocrystalline cellulose extraction. Can J Chem Eng 88(3):392–402

Jonoobi M, Oladi R, Davoudpour Y, Oksman K, Dufresne A, Hamzeh Y, Davoodi R (2015) Different preparation methods and properties of nanostructured cellulose from various natural resources and residues: a review. Cellulose 22(2):935–969

Kelly JA, Shukaliak AM, Cheung CCY, Shopsowitz KE, Hamad WY, MacLachlan MJ (2013) Responsive photonic hydrogels based on nanocrystalline cellulose. Angew Chem Int Ed 52(34):8912–8916

Kim J-H, Shim BS, Kim HS, Lee Y-J, Min S-K, Jang D, Abas Z, Kim J (2015) Review of nanocellulose for sustainable future materials. Int J Precis Eng Manuf Green Technol 2(2):197–213

Kurihara T, Isogai A (2014) Properties of poly(acrylamide)/TEMPO-oxidized cellulose nanofibril composite films. Cellulose 21(1):291–299

Lacerda TM, Zarnbon MD, Frollini E (2015) Oxalic acid as a catalyst for the hydrolysis of sisal pulp. Ind Crops Prod 71:163–172

Li B, Xu W, Kronlund D, Maattanen A, Liu J, Smatt J-H, Peltonen J, Willfor S, Mu X, Xu C (2015) Cellulose nanocrystals prepared via formic acid hydrolysis followed by TEMPO-mediated oxidation. Carbohydr Polym 133:605–612

Lin N, Dufresne A (2014) Surface chemistry, morphological analysis and properties of cellulose nanocrystals with gradiented sulfation degrees. Nanoscale 6(10):5384–5393

Liu Y, Wang H, Yu G, Yu Q, Li B, Mu X (2014) A novel approach for the preparation of nanocrystalline cellulose by using phosphotungstic acid. Carbohydr Polym 110:415–422

Lu P, Hsieh Y-L (2010) Preparation and properties of cellulose nanocrystals: Rods, spheres, and network. Carbohydr Polym 82(2):329–336

Lu Q, Tang L, Lin F, Wang S, Chen Y, Chen X, Huang B (2014) Preparation and characterization of cellulose nanocrystals via ultrasonication-assisted FeCl3-catalyzed hydrolysis. Cellulose 21(5):3497–3506

Lu Q, Lin W, Tang L, Wang S, Chen X, Huang B (2015) A mechanochemical approach to manufacturing bamboo cellulose nanocrystals. J Mater Sci 50(2):611–619

Luzi F, Fortunati E, Puglia D, Lavorgna M, Santulli C, Kenny JM, Torre L (2014) Optimized extraction of cellulose nanocrystals from pristine and carded hemp fibres. Ind Crops Prod 56:175–186

Mansikkamaki P, Lahtinen M, Rissanen K (2005) Structural changes of cellulose crystallites induced by mercerisation in different solvent systems; determined by powder X-ray diffraction method. Cellulose 12(3):233–242

Mathew AP, Oksman K, Karim Z, Liu P, Khan SA, Naseri N (2014) Process scale up and characterization of wood cellulose nanocrystals hydrolysed using bioethanol pilot plant. Ind Crops Prod 58:212–219

Mendez J, Annamalai PK, Eichhorn SJ, Rusli R, Rowan SJ, Foster EJ, Weder C (2011) Bioinspired mechanically adaptive polymer nanocomposites with water-activated shape-memory effect. Macromolecules 44(17):6827–6835

Moon RJ, Martini A, Nairn J, Simonsen J, Youngblood J (2011) Cellulose nanomaterials review: structure, properties and nanocomposites. Chem Soc Rev 40:3941–3994

Peyre J, Paakkonen T, Reza M, Kontturi E (2015) Simultaneous preparation of cellulose nanocrystals and micron-sized porous colloidal particles of cellulose by TEMPO-mediated oxidation. Green Chem 17(2):808–811

Roman M, Winter WT (2004) Effect of sulfate groups from sulfuric acid hydrolysis on the thermal degradation behavior of bacterial cellulose. Biomacromolecules 5(5):1671–1677

Sacui IA, Nieuwendaal RC, Burnett DJ, Stranick SJ, Jorfi M, Weder C, Foster EJ, Olsson RT, Gilman JW (2014) Comparison of the properties of cellulose nanocrystals and cellulose nanofibrils isolated from bacteria, tunicate, and wood processed using acid, enzymatic, mechanical, and oxidative methods. ACS Appl Mater Interfaces 6(9):6127–6138

Schyrr B, Pasche S, Voirin G, Weder C, Simon YC, Foster EJ (2014) Biosensors based on porous cellulose nanocrystal-poly(vinyl alcohol) scaffolds. ACS Appl Mater Interfaces 6(15):12674–12683

Segal L, Creely JJ, Martin AE, Conrad CM (1959) An empirical method for estimating the degree of crystallinity of native cellulose using the X-ray diffractometer. Textile Res J 29(10):786–794

Sihtola H, Kyrklund B, Laamanen L, Palenius I (1963) Comparison and conversion of viscosity and DP-values determined by different methods. Paperi ja Puu 45:225–232

Spinella S, Lo Re G, Liu B, Dorgan J, Habibi Y, Leclere P, Raquez J-M, Dubois P, Gross RA (2015) Polylactide/cellulose nanocrystal nanocomposites: efficient routes for nanofiber modification and effects of nanofiber chemistry on PLA reinforcement. Polymer 65:9–17

Taheri A, Mohammadi M (2015) The use of cellulose nanocrystals for potential application in topical delivery of hydroquinone. Chem Biol Drug Des 86(1):882–886

Tang L, Huang B, Lu Q, Wang S, Ou W, Lin W, Chen X (2013) Ultrasonication-assisted manufacture of cellulose nanocrystals esterified with acetic acid. Bioresour Technol 127:100–105

van den Berg O, Capadona JR, Weder C (2007) Preparation of homogeneous dispersions of tunicate cellulose whiskers in organic solvents. Biomacromolecules 8(4):1353–1357

Wang N, Ding EY, Cheng RS (2007) Thermal degradation behaviors of spherical cellulose nanocrystals with sulfate groups. Polymer 48(12):3486–3493

Wang QQ, Zhu JY, Reiner RS, Verrill SP, Baxa U, McNeil SE (2012) Approaching zero cellulose loss in cellulose nanocrystal (CNC) production: recovery and

characterization of cellulosic solid residues (CSR) and CNC. Cellulose 19(6):2033–2047

Wang QQ, Zhu JY, Considine JM (2013) Strong and optically transparent films prepared using cellulosic solid residue (CSR) recovered from cellulose nanocrystals (CNC) production waste stream. ACS Appl Mater Interfaces 5(7):2527–2534

Wang Q, Zhao X, Zhu JY (2014) Kinetics of strong acid hydrolysis of a bleached kraft pulp for producing cellulose nanocrystals (CNCs). Ind Eng Chem Res 53(27):11007–11014

Wang W, Mozuch MD, Sabo RC, Kersten P, Zhu JY, Jin Y (2015) Production of cellulose nanofibrils from bleached eucalyptus fibers by hyperthermostable endoglucanase treatment and subsequent microfluidization. Cellulose 22:351–361

Wang R, Chen L, Zhu JY, Yang R (2017) Tailored and integrated production of carboxylated cellulose nanocrystals (CNC) with nanofibrils (CNF) through maleic acid hydrolysis. ChemNanoMat. doi:10.1002/cnma.201700015

Xiang ZY, Gao WH, Chen LH, Lan W, Zhu JY, Runge T (2016) A comparison of cellulose nanofibrils produced from Cladophora glomerata algae and bleached eucalyptus pulp. Cellulose 23(1):493–503

Xu XZ, Liu F, Jiang L, Zhu JY, Haagenson D, Wiesenborn DP (2013) Cellulose nanocrystals vs. cellulose nanofibrils: a comparative study on their microstructures and effects as polymer reinforcing agents. ACS Appl Mater Interfaces 5(8):2999–3009

Xu X, Wang H, Jiang L, Wang X, Payne SA, Zhu JY, Li R (2014) Comparison between cellulose nanocrystal and cellulose nanofibril reinforced poly(ethylene oxide) nanofibers and their novel shish-kebab-like crystalline structures. Macromolecules 47(10):3409–3416

Xu XZ, Zhou J, Jiang L, Lubineau G, Ng T, Ooi BS, Liao HY, Shen C, Chen L, Zhu JY (2016) Highly transparent, low-haze, hybrid cellulose nanopaper as electrodes for flexible electronics. Nanoscale 8(24):12294–12306

Yu H, Qin Z, Liang B, Liu N, Zhou Z, Chen L (2013) Facile extraction of thermally stable cellulose nanocrystals with a high yield of 93% through hydrochloric acid hydrolysis under hydrothermal conditions. J Mater Chem A 1(12):3938–3944

Yu H-Y, Chen G-Y, Wang Y-B, Yao J-M (2015) A facile one-pot route for preparing cellulose nanocrystal/zinc oxide nanohybrids with high antibacterial and photocatalytic activity. Cellulose 22(1):261–273

Zhang S, Winestrand S, Guo X, Chen L, Hong F, Jonsson LJ (2014) Effects of aromatic compounds on the production of bacterial nanocellulose by Gluconacetobacter xylinus. Microb Cell Fact 13:62

Zhang K, Sun P, Liu H, Shang S, Song J, Wang D (2016a) Extraction and comparison of carboxylated cellulose nanocrystals from bleached sugarcane bagasse pulp using two different oxidation methods. Carbohydr Polym 138:237–243

Zhang Q, Bao W, Gong A, Gong T, Ma D, Wan J, Dai J, Munday JN, He JH, Hu L et al (2016b) A highly sensitive, highly transparent, gel-gated MoS2 phototransistor on biodegradable nanopaper. Nanoscale 8(29):14237–14242

Zhu JY, Sabo R, Luo X (2011) Integrated production of nanofibrillated cellulose and cellulosic biofuel (ethanol) by enzymatic fractionation of wood fibers. Green Chem 13(5):1339–1344

Zhu H, Fang Z, Wang Z, Dai J, Yao Y, Shen F, Preston C, Wu W, Peng P, Jang N et al (2016) Extreme light management in mesoporous wood cellulose paper for optoelectronics. ACS Nano 10(1):1369–1377